Rapid Communications

Towards predictive many-body calculations of phonon-limited carrier mobilities in semiconductors

Samuel Poncé,[1] Elena R. Margine,[2] and Feliciano Giustino[1,*]
[1]*Department of Materials, University of Oxford, Parks Road, Oxford, OX1 3PH, United Kingdom*
[2]*Department of Physics, Binghamton University-SUNY, Binghamton, New York 13902, USA*

(Received 15 October 2017; published 27 March 2018)

We probe the accuracy limit of *ab initio* calculations of carrier mobilities in semiconductors, within the framework of the Boltzmann transport equation. By focusing on the paradigmatic case of silicon, we show that fully predictive calculations of electron and hole mobilities require many-body quasiparticle corrections to band structures and electron-phonon matrix elements, the inclusion of spin-orbit coupling, and an extremely fine sampling of inelastic scattering processes in momentum space. By considering all these factors we obtain excellent agreement with experiment, and we identify the band effective masses as the most critical parameters to achieve predictive accuracy. Our findings set a blueprint for future calculations of carrier mobilities, and pave the way to engineering transport properties in semiconductors by design.

DOI: 10.1103/PhysRevB.97.121201

During the last decade, materials design guided by first-principles calculations has emerged as a powerful research strategy. Nowadays it is often possible to accurately predict ground-state properties of new materials *in silico*. This information can be used to screen for promising new materials [1,2]. At variance with ground-state properties, the prediction and screening of materials properties involving electronic excitations is still in its infancy. For example, charge and heat transport coefficients are typically evaluated using a combination of *ab initio* and semiempirical approaches [3–7]. The reasons for this lag are that the evaluation of transport coefficients is considerably more challenging than total energies, the computational infrastructure is not yet fully developed, and the lack of a clear set of reference data for validation and verification [8].

In this work, we focus on phonon-limited carrier mobilities in semiconductors. The theoretical framework for calculating mobilities is well established, and is rooted in the Boltzmann transport equation (BTE), as described in Refs. [9–11]. The BTE is a semiclassical, quasiparticle theory of electron transport, which can be rigorously derived from a many-body quantum-field theoretic framework by neglecting two-particle correlations [12]. The key ingredients are the electronic band structures, the phonon dispersion relations, and the electron-phonon matrix elements. The calculations of these quantities have reached maturity [13], therefore there should be no fundamental obstacles towards predicting mobilities. However, already for the most studied semiconductor, silicon, one finds that (i) calculations of carrier mobilities are scarce, (ii) there is considerable scatter in the calculated data, and (iii) reproducing measured mobilities remains a challenge. For example, Refs. [14–17] calculate intrinsic electron mobilities at room temperature $\mu_e = 1550$, 1750, 1860, and 1970 $\mathrm{cm}^2/\mathrm{V\,s}$, respectively, while experiments are in the range 1300–1450 $\mathrm{cm}^2/\mathrm{V\,s}$ [18–20].

Motivated by these considerations, here we set out to clarify the accuracy limit and the predictive power of *ab initio* mobility calculations based on the BTE. We show that in order to correctly reproduce experimental data we need to take into account GW quasiparticle corrections to the band structures and the electron-phonon matrix elements, to include the spin-orbit splitting of the valence bands, and to properly converge the integrals over the Brillouin zone. We also find that accurate band effective masses are absolutely critical to reproduce measured mobilities. By considering all these aspects, we succeed in reproducing measured data with high accuracy, thus establishing unambiguously the predictive power of the *ab initio* BTE.

In a semiconductor the steady-state electric current $\mathbf{J}$ is related to the driving electric field $\mathbf{E}$ via the mobility tensors as $J_\alpha = e\,(n_\mathrm{e}\,\mu_{\mathrm{e},\alpha\beta} + n_\mathrm{h}\mu_{\mathrm{h},\alpha\beta})E_\beta$, where Greek indices denote Cartesian coordinates. In this expression $\mu_{\mathrm{e},\alpha\beta}$,$n_\mathrm{e}$ and $\mu_{\mathrm{h},\alpha\beta}$,$n_\mathrm{h}$ are the mobility and particle density of electrons and holes, respectively. Within Boltzmann's transport formalism [9] the current density is expressed as $J_\alpha = -e\,\Omega^{-1}\sum_n \Omega_{\mathrm{BZ}}^{-1}\int d\mathbf{k}\, f_{n\mathbf{k}} v_{n\mathbf{k},\alpha}$, where Ω and Ω_{BZ} are the volume of the crystalline unit cell and the first Brillouin zone, respectively. The occupation factor $f_{n\mathbf{k}}$ plays the role of a statistical distribution function, and reduces to the Fermi-Dirac distribution $f^0_{n\mathbf{k}}$ in the absence of the electric field. The band velocity is given by $v_{n\mathbf{k},\alpha} = \hbar^{-1}\partial\varepsilon_{n\mathbf{k}}/\partial k_\alpha$, where $\varepsilon_{n\mathbf{k}}$ is the single-particle electron eigenvalue for the state $|n\mathbf{k}\rangle$.

Using these definitions, the electron mobility is obtained via the derivative of the current with respect to the electric field: $\mu_{\mathrm{e},\alpha\beta} = -\sum_{n\in\mathrm{CB}}\int d\mathbf{k}\, v_{n\mathbf{k},\alpha}\partial_{E_\beta} f_{n\mathbf{k}} / \sum_{n\in\mathrm{CB}}\int d\mathbf{k}\, f^0_{n\mathbf{k}}$. Here the summations are restricted to the conduction bands, and ∂_{E_β} is short for $\partial/\partial E_\beta$. An analogous expression holds for holes. From this expression we see that in order to calculate mobilities we need to evaluate $\partial_{E_\beta} f_{n\mathbf{k}}$, which is the linear response of the distribution function $f_{n\mathbf{k}}$ to the electric field

*feliciano.giustino@materials.ox.ac.uk

E. This quantity can be computed starting from the BTE [9]:

$$
\begin{aligned}
(-e)\mathbf{E}\cdot\frac{1}{\hbar}\frac{\partial f_{n\mathbf{k}}}{\partial \mathbf{k}} = \frac{2\pi}{\hbar}\sum_{m\nu}\int\frac{d\mathbf{q}}{\Omega_{\mathrm{BZ}}}|g_{mn\nu}(\mathbf{k},\mathbf{q})|^2 \\
\times\{(1-f_{n\mathbf{k}})f_{m\mathbf{k}+\mathbf{q}}\delta(\varepsilon_{n\mathbf{k}}-\varepsilon_{m\mathbf{k}+\mathbf{q}}+\hbar\omega_{\mathbf{q}\nu})(1+n_{\mathbf{q}\nu}) \\
+(1-f_{n\mathbf{k}})f_{m\mathbf{k}+\mathbf{q}}\delta(\varepsilon_{n\mathbf{k}}-\varepsilon_{m\mathbf{k}+\mathbf{q}}-\hbar\omega_{\mathbf{q}\nu})n_{\mathbf{q}\nu} \\
-f_{n\mathbf{k}}(1-f_{m\mathbf{k}+\mathbf{q}})\delta(\varepsilon_{n\mathbf{k}}-\varepsilon_{m\mathbf{k}+\mathbf{q}}-\hbar\omega_{\mathbf{q}\nu})(1+n_{\mathbf{q}\nu}) \\
-f_{n\mathbf{k}}(1-f_{m\mathbf{k}+\mathbf{q}})\delta(\varepsilon_{n\mathbf{k}}-\varepsilon_{m\mathbf{k}+\mathbf{q}}+\hbar\omega_{\mathbf{q}\nu})n_{\mathbf{q}\nu}\}. \qquad (1)
\end{aligned}
$$

The left-hand side of Eq. (1) represents the collisionless term of Boltzmann's equation for a uniform and constant electric field, in the absence of temperature gradients and magnetic fields; the right-hand side represents the modification of the distribution function arising from electron-phonon scattering in and out of the state $|n\mathbf{k}\rangle$, via emission or absorption of phonons with frequency $\omega_{\mathbf{q}\nu}$, wave vector $\mathbf{q}$, and branch index ν [10]. $n_{\mathbf{q}\nu}$ is the Bose-Einstein distribution function. The matrix elements $g_{mn\nu}(\mathbf{k},\mathbf{q})$ in Eq. (1) are the probability amplitude for scattering from an initial electronic state $|n\mathbf{k}\rangle$ into a final state $|m\mathbf{k}+\mathbf{q}\rangle$ via a phonon $|\mathbf{q}\nu\rangle$, as obtained from density-functional perturbation theory [13,21]. By taking derivatives of Eq. (1) with respect to **E** we obtain an explicit expression for the variation $\partial_{E_\beta} f_{n\mathbf{k}}$:

$$
\begin{aligned}
\partial_{E_\beta} f_{n\mathbf{k}} = e\frac{\partial f^0_{n\mathbf{k}}}{\partial\varepsilon_{n\mathbf{k}}}v_{n\mathbf{k},\beta}\tau^0_{n\mathbf{k}}+\frac{2\pi\tau^0_{n\mathbf{k}}}{\hbar}\sum_{m\nu}\int\frac{d\mathbf{q}}{\Omega_{\mathrm{BZ}}}|g_{mn\nu}(\mathbf{k},\mathbf{q})|^2 \\
\times\left[\left(1+n_{\mathbf{q}\nu}-f^0_{n\mathbf{k}}\right)\delta(\varepsilon_{n\mathbf{k}}-\varepsilon_{m\mathbf{k}+\mathbf{q}}+\hbar\omega_{\mathbf{q}\nu})\right. \\
\left.+\left(n_{\mathbf{q}\nu}+f^0_{n\mathbf{k}}\right)\delta(\varepsilon_{n\mathbf{k}}-\varepsilon_{m\mathbf{k}+\mathbf{q}}-\hbar\omega_{\mathbf{q}\nu})\right]\partial_{E_\beta}f_{m\mathbf{k}+\mathbf{q}}, \qquad (2)
\end{aligned}
$$

having defined the relaxation time:

$$
\begin{aligned}
\frac{1}{\tau^0_{n\mathbf{k}}} = \frac{2\pi}{\hbar}\sum_{m\nu}\int\frac{d\mathbf{q}}{\Omega_{\mathrm{BZ}}}|g_{mn\nu}(\mathbf{k},\mathbf{q})|^2 \\
\times\left[\left(1-f^0_{m\mathbf{k}+\mathbf{q}}+n_{\mathbf{q}\nu}\right)\delta(\varepsilon_{n\mathbf{k}}-\varepsilon_{m\mathbf{k}+\mathbf{q}}-\hbar\omega_{\mathbf{q}\nu})\right. \\
\left.+\left(f^0_{m\mathbf{k}+\mathbf{q}}+n_{\mathbf{q}\nu}\right)\delta(\varepsilon_{n\mathbf{k}}-\varepsilon_{m\mathbf{k}+\mathbf{q}}+\hbar\omega_{\mathbf{q}\nu})\right]. \qquad (3)
\end{aligned}
$$

Equation (2) is the linearized BTE and is valid under the assumption that the energy gained by a carrier accelerated by the electric field over the mean free path is much smaller than the thermal energy, $eE_\beta v_{n\mathbf{k},\beta}\tau^0_{n\mathbf{k}} \ll k_B T$; this assumption is verified in most semiconductors under standard operating conditions. This equation needs to be solved self-consistently for $\partial_{E_\beta} f_{n\mathbf{k}}$, and is also referred to as the iterative BTE (IBTE). A simpler approach consists in neglecting the integral on the right-hand side of Eq. (2). In this case we obtain the variation $\partial_{E_\beta} f_{n\mathbf{k}}$ without solving iteratively. It can be shown that the relaxation time $\tau^0_{n\mathbf{k}}$ is related to the imaginary part of the Fan-Migdal electron self-energy [13] via $1/\tau^0_{n\mathbf{k}} = 2\,\mathrm{Im}\,\Sigma^{\mathrm{FM}}_{n\mathbf{k}}$. Based on this analogy, in the following we refer to the approximation of neglecting the integral in Eq. (2) as the "self-energy relaxation time approximation" (SERTA). In this approximation the mobility takes the simple form

$$
\mu_{\mathrm{e},\alpha\beta} = \frac{-e}{n_{\mathrm{e}}\,\Omega}\sum_{n\in\mathrm{CB}}\int\frac{d\mathbf{k}}{\Omega_{\mathrm{BZ}}}\frac{\partial f^0_{n\mathbf{k}}}{\partial\varepsilon_{n\mathbf{k}}}v_{n\mathbf{k},\alpha}v_{n\mathbf{k},\beta}\tau^0_{n\mathbf{k}}. \qquad (4)
$$

We perform calculations within density-functional theory (DFT), plane waves, and pseudopotentials using the EPW code [22] of the QUANTUM ESPRESSO distribution [23], in conjunction with the WANNIER90 library [24]. This approach employs a generalized Wannier-Fourier interpolation technique [25] in order to obtain electron eigenvalues, phonon eigenfrequencies, and electron-phonon matrix elements on dense Brillouin-zone grids by means of maximally localized Wannier functions [26]. A fine sampling of the Brillouin zone is required because, at finite temperature, the Fermi level lies within the band gap, therefore we need to sample scattering processes taking place in the tails of the Fermi-Dirac distribution. In our calculations the Fermi level is determined in such a way that the net charge density at a given temperature, $n_{\mathrm{e}} - n_{\mathrm{h}}$, equals the doping level ($n_{\mathrm{e}} = n_{\mathrm{h}}$ for an intrinsic material). We now analyze in turn the key ingredients when calculating mobilities. We consider the paradigmatic case of silicon, for which extensive experimental data are available.

Brillouin-zone sampling. We find that in order to obtain reliable intrinsic mobilities it is necessary to employ extremely fine quasirandom grids, with a densified sampling around the band extrema [27]. Convergence of mobility values to within 0.5% is reached when using grids with 85 K inequivalent **k** points and 200 K inequivalent **q** points [white dot in Supplemental Material Fig. S1(a) [27]]. Subsequent calculations in this Rapid Communication are performed using these grids. In Supplemental Material Fig. S1(b) we compare calculations of the intrinsic mobility of silicon within the SERTA and the IBTE approaches. We find that the iterative solution of Eq. (2) leads to converged values which are 6% higher than the SERTA result for electrons, and 1% lower for holes. Since the IBTE is drastically more expensive because it requires homogeneous and commensurate grids [15,16], in the following discussion we focus on SERTA calculations. We use a finite broadening of 5 meV to evaluate the Dirac delta function in Eq. (3). The sensitivity of the results to the broadening parameter is analyzed in the Supplemental Material [27].

Exchange and correlation. In order to investigate the effect of the DFT exchange and correlation we perform calculations within both the local density approximation (LDA) [28,29] and the generalized gradient approximation of Perdew, Burke, and Ernzerhof (PBE) [30], using scalar-relativistic pseudopotentials [31]. Figure 1 shows that the intrinsic mobilities at 300 K differ by 16% between LDA and PBE for electrons, and by 3% for holes. Closer inspection shows that these differences arise primarily from the optimized lattice parameters obtained with these functionals ($a = 5.40$ Å in LDA and 5.47 Å in PBE). In fact, when using the experimental lattice parameter ($a = 5.43$ Å) the deviation between LDA and PBE mobilities reduces to 0.4% for electrons and 2% for holes (Fig. 1). These results indicate that the choice of exchange and correlation is not critical so long as accurate lattice parameters are employed.

Spin-orbit coupling. Spin-orbit interactions in silicon are very weak [32], therefore relativistic effects are usually neglected. However, here we find that spin-orbit coupling is important for predictive calculations, yielding hole mobilities 9% higher than nonrelativistic calculations (Fig. 1). This effect can be understood by considering the band structures in Fig. 2(b). The spin-orbit interaction splits the sixfold degenerate states

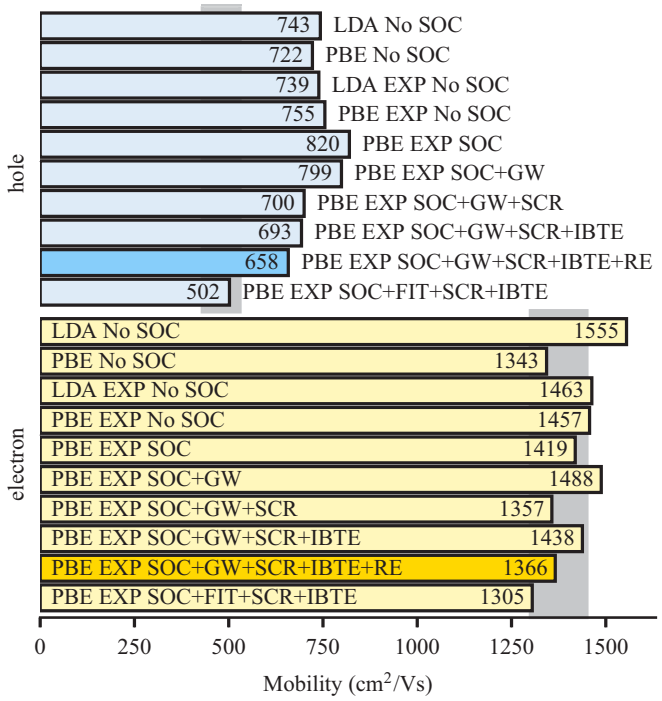

FIG. 1. Intrinsic electron and hole mobilities of silicon at 300 K, calculated using various levels of theory. The complexity of the theory increases as we move down the sequence of bars. The range of measured mobilities is indicated in light-gray vertical bars. Our most accurate theoretical predictions are $\mu_e = 1366$ cm^2/V s and $\mu_h = 658$ cm^2/V s; by replacing the GW hole effective mass with the experimental value we obtain $\mu_e = 502$ cm^2/V s, in much better agreement with experiment. Key: SOC, spin-orbit coupling; EXP, experimental lattice parameter; GW, calculations including quasiparticle corrections; SCR, electron-phonon coupling with corrected screening; IBTE, iterative Boltzmann transport equation; RE, change of effective mass due to electron-phonon renormalization; FIT, band structures calculated from the measured effective masses.

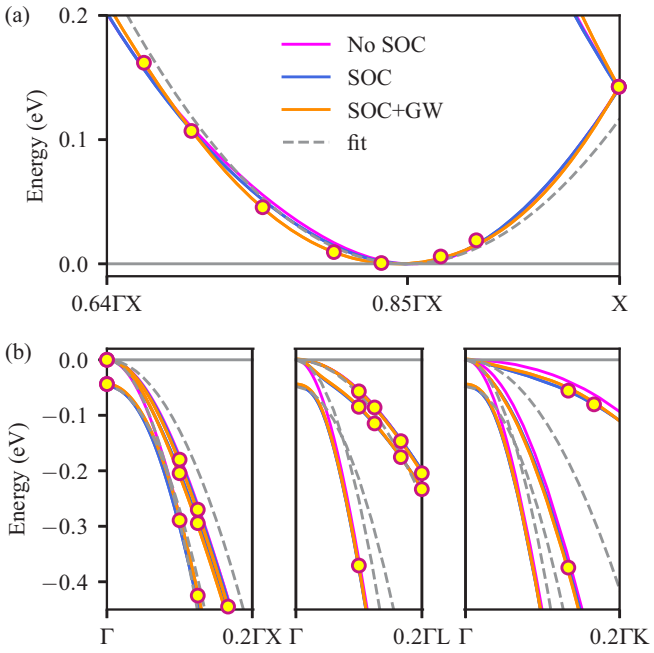

FIG. 2. (a) Conduction bands of silicon calculated within scalar-relativistic PBE (gray), fully relativistic PBE (blue), the GW method (orange), and parabolic fit with measured effective masses (dashed). The zero of the energy axis is set to the conduction band minimum for clarity. (b) Valence bands of silicon, calculated within the same approximations as for (a), and shown using the same color code. The zero of the energy axis is set to the valence band top. In all panels the dots indicate explicit GW calculations carried out using uniform grids containing $12 \times 12 \times 12$ to $20 \times 20 \times 20$ points. The GW bands in orange are obtained via Wannier interpolation.

at the top of the valence bands, leading to the formation of two doubly degenerate light-hole and heavy-hole bands, and one doubly degenerate split-off hole band. As a result the effective mass of the light hole decreases (see Supplemental Material Table S1 [27]), leading to a higher mobility. On the other hand, Fig. 2(a) shows that the conduction band bottom is relatively unaffected by spin-orbit coupling, and correspondingly the effect on the electron mobility is less pronounced (2.7%).

Many-body quasiparticle corrections. Given the sensitivity of the calculated mobilities to the band extrema, we investigate the effect of many-body correlations within the GW quasiparticle approximation. To obtain quasiparticle energies we use the YAMBO code [33]; the values calculated on a $12 \times 12 \times 12$ uniform grid are then interpolated using the EPW code. Figure 2 shows the modification to the band extrema resulting from quasiparticle corrections. In the case of the valence bands, quasiparticle corrections increase the mass of the light holes (see Supplemental Material Table S1 [27]); as a result the hole mobility decreases by 3%, as shown in Fig. 1. The opposite effect is observed for the conduction bands where the electron mobility is increased by 5%.

Corrections to the DFT screening. Another source of error in the DFT calculations of carrier mobilities is the over-screening of the electron-phonon matrix elements $g_{mnv}(\mathbf{k},\mathbf{q})$ associated with the DFT band gap problem [13]. In fact, in the case of silicon DFT yields a static dielectric constant $\epsilon^0_{\rm DFT} = 12.89$, which is higher than the measured value $\epsilon^0_{\rm expt} = 11.94$ [20]. In order to overcome this issue it is necessary to modify the screening in the calculation of phonon dispersion relations. Since this is computationally prohibitive, here we take a simpler approach and renormalize the matrix elements as follows: $g'_{mnv}(\mathbf{k},\mathbf{q}) = g_{mnv}(\mathbf{k},\mathbf{q})[\epsilon_{\rm DFT}(|\mathbf{q}|)/\epsilon_{\rm expt}(|\mathbf{q}|)]$. Here $\epsilon_{\rm expt}$ is meant to be the most accurate description of the screening that we can afford, and we are neglecting local-field effects which should yield an error on the order of a few percent [40]. For practical purposes we replace the dielectric functions by an analytic expression [41], where the only input parameter is the head of the dielectric matrix. The validity of this procedure is demonstrated in Supplemental Material Fig. S3 [27] using explicit calculations in the random-phase approximation. This correction to the matrix elements leads to a decrease of the electron and hole mobilities by 8.8% and 12.4%, respectively, as shown in Fig. 1.

Thermal expansion and electron-phonon renormalization. We computed the effect of thermal lattice expansion on the DFT eigenenergies using the THERMO_PW code [42] within the quasiharmonic approximation and concluded that this

effect is negligible (see Supplemental Material Fig. S6 [27]). We also determined the electron-phonon renormalization of the effective masses using data from Ref. [43]. This effect increases the masses by ∼3%, and results in a decrease of the mobilities by ∼5%.

After considering all the effects discussed so far, and after accounting for the corrections to the SERTA results arising from the solution of the complete IBTE, our most accurate theoretical mobilities at 300 K are $\mu_e = 1366\ \mathrm{cm}^2/\mathrm{V\,s}$ and $\mu_h = 658\ \mathrm{cm}^2/\mathrm{V\,s}$. These values are to be compared to the measured drift mobilities $\mu_e^{\mathrm{expt}} = 1350$–$1450\ \mathrm{cm}^2/\mathrm{V\,s}$ [36,37,39,44] and $\mu_h^{\mathrm{expt}} = 445$–$510\ \mathrm{cm}^2/\mathrm{V\,s}$ [36,37,44,45] (Fig. 1). From the comparison with experiment we see that by pushing the theory to its limits we can obtain electron mobilities in very good agreement with experiment. On the contrary, the hole mobility is still approximately 30% above the measured range. This discrepancy can be traced back to the underestimation of the [100] heavy-hole effective masses within the GW approximation. In fact, by repeating the calculation using the experimental hole effective mass instead of the GW mass, we obtain a hole mobility $\mu_h' = 502\ \mathrm{cm}^2/\mathrm{V\,s}$, this time in very good agreement with experiment as shown in Fig. 1. This result leads us to conclude that the effective mass plays an absolutely critical role in mobility calculations. Our finding can be understood by considering that the mobility varies with the effective mass as $\mu = (m^*)^{-p}$ with p being a coefficient between 1 and 2.5 [46–48]; as a result a 20% error in the effective mass leads to an error in the mobility of up to 60%. This finding highlights the critical role of accurate calculations of quasiparticle band structures, and raises the question on whether the standard GW method and pseudopotential calculations (see Supplemental Material Table S2) are sufficient for delivering predictive mobilities.

Using the best possible computational setup we can now compare our calculations with experiment over a range of temperatures and doping levels. Figure 3(a) shows the intrinsic electron and hole mobilities of silicon between 100 and 500 K. In the case of the hole mobilities we show both our best *ab initio* results (solid line), as well as those recalculated using the experimental effective masses (dashed line). Overall, the agreement between our calculations and experiment is very good throughout the entire temperature range. Figure 3(b) shows a comparison between calculated and measured mobilities at 300 K, as a function of carrier concentration between 10^{15} and $10^{19}\ \mathrm{cm}^{-3}$. In this case, in addition to the *ab initio* electron-phonon scattering, we used the semiempirical model of Brooks and Herring with the Long-Norton correction [38,39] to account for impurity scattering (see Supplemental Material for details [27]). Also in this case we find very good agreement with experiment, although the contribution of impurity scattering is evaluated semiempirically.

In conclusion, we pushed the accuracy of transport calculations within the BTE formalism to its limits, and we demonstrated that this approach can deliver predictive accuracy for a prototypical semiconductor. Our findings raise two important questions for future work on transport in semiconductors: (i) the present formalism yields results which fall within the experimental uncertainty. In order to enable further progress in this area it will be important to produce high-quality experimental data from single-crystal samples. (ii) An unexpected challenge that we faced is to perform accurate *ab initio* calculations of effective masses. Going forward it will be important to establish whether the GW method and pseudopotential calculations can provide effective masses with the accuracy required for predictive mobility calculations. Meanwhile, the present work opens the way to predictive calculations of mobilities and lays the groundwork for the *ab initio* design of semiconductor devices.

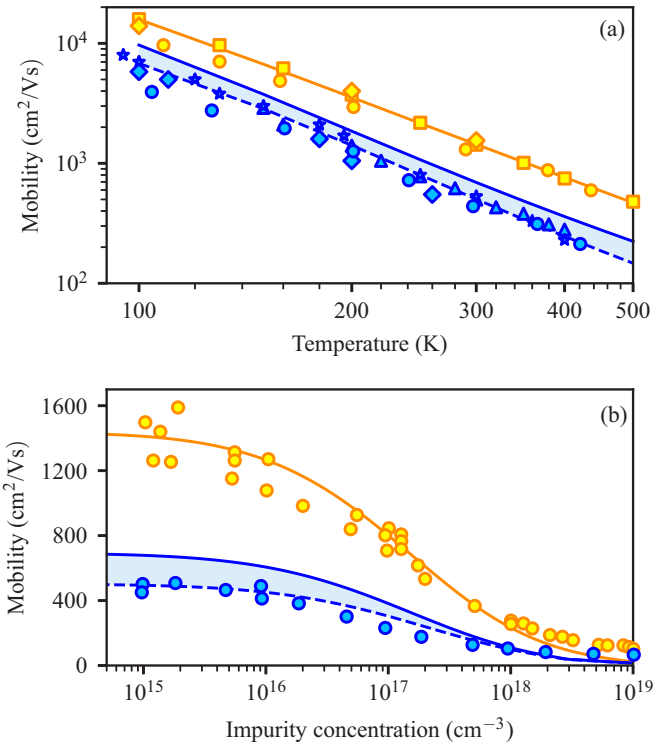

FIG. 3. (a) Comparison between calculated and measured intrinsic (low carrier concentration $\leqslant 10^{15}\ \mathrm{cm}^{-3}$) electron and hole mobilities of silicon, as a function of temperature. The calculations are performed using our best computational setup. The blue lines are for holes and the orange line is for electrons. In the case of holes we show both our best *ab initio* calculations (solid blue), and the results obtained by setting the hole effective mass to the experimental value (dashed blue). The shading is a guide to the eye. Experiments are from [34] (△), [35] (◇), [36] (⋆), [37] (○), and [19] (□). (b) Comparison between calculated and measured electron and hole mobilities of silicon at 300 K, as a function of carrier concentration, using the same color code as in (a). Experimental data are from [37] (○). The impurity scattering is included via the model of Brooks and Herring with the Long-Norton correction [38,39] as described in the Supplemental Material [27].

Note added. Recently, a related calculation for Si was reported, where the authors found a significant increase in Si hole mobility with spin-orbit coupling (SOC) and no effect from SOC on the electron mobility in line with our results [49].

Acknowledgments. We acknowledge fruitful discussions with C. Verdi, M. Schlipf, and W. Li. This work was supported by the Leverhulme Trust (Grant No. RL-2012-001), the UK EPSRC Research Council (Grants No. EP/J009857/1 and No. EP/M020517/1), the EU H2020 programme under Grant No. 696656 GrapheneCore1, the University of Oxford Advanced

Research Computing (ARC) facility [50], the ARCHER UK National Supercomputing Service under the AMSEC and CTOA projects, PRACE DECI-13 resource Cartesius at SURFsara, and the PRACE DECI-14 resource Abel at UiO. E.R.M. acknowledges support from the NSF under Award No. OAC-1740263.

[1] S. Curtarolo, G. L. W. Hart, M. B. Nardelli, N. Mingo, S. Sanvito, and O. Levy, Nat. Mater. **12**, 191 (2013).
[2] A. Jain, Y. Shin, and K. A. Persson, Nat. Rev. Mater. **1**, 1 (2016).
[3] S. Wang, Z. Wang, W. Setyawan, N. Mingo, and S. Curtarolo, Phys. Rev. X **1**, 021012 (2011).
[4] X. Chen, D. Parker, and D. J. Singh, Sci. Rep. **3**, 3168 (2013).
[5] G. Hautier, A. Miglio, G. Ceder, G.-M. Rignanese, and X. Gonze, Nat. Commun. **4**, 2292 (2013).
[6] B. Xu and M. J. Verstraete, Phys. Rev. Lett. **112**, 196603 (2014).
[7] K. Krishnaswamy, B. Himmetoglu, Y. Kang, A. Janotti, and C. G. Van de Walle, Phys. Rev. B **95**, 205202 (2017).
[8] K. Lejaeghere, G. Bihlmayer, T. Björkman, P. Blaha, S. Blügel, V. Blum, D. Caliste, I. E. Castelli, S. J. Clark, A. Dal Corso, S. de Gironcoli, T. Deutsch, J. K. Dewhurst, I. Di Marco, C. Draxl, M. Dułak, O. Eriksson, J. A. Flores-Livas, K. F. Garrity, L. Genovese *et al.*, Science **351**, aad3000 (2016).
[9] J. Ziman, *Electrons and Phonons*, edited by N. F. Mott, E. C. Bullard, and D. H. Wilkinson (Oxford University Press, Oxford, 1960).
[10] G. Grimvall, *The Electron-Phonon Interaction in Metals* (North-Holland, Amsterdam, 1981).
[11] G. D. Mahan, *Many-Particle Physics* (Springer, New York, 2000).
[12] L. P. Kadanoff and G. Baym, *Quantum Statistical Mechanics* (Benjamin, New York, 1962).
[13] F. Giustino, Rev. Mod. Phys. **89**, 015003 (2017).
[14] J. Zhou, B. Liao, B. Qiu, S. Huberman, K. Esfarjani, M. S. Dresselhaus, and G. Chen, Proc. Natl. Acad. Sci. USA **112**, 14777 (2015).
[15] M. Fiorentini and N. Bonini, Phys. Rev. B **94**, 085204 (2016).
[16] W. Li, Phys. Rev. B **92**, 075405 (2015).
[17] O. D. Restrepo, K. Varga, and S. T. Pantelides, Appl. Phys. Lett. **94**, 212103 (2009).
[18] C. Canali, C. Jacoboni, F. Nava, G. Ottaviani, and A. Alberigi-Quaranta, Phys. Rev. B **12**, 2265 (1975).
[19] P. Norton, T. Braggins, and H. Levinstein, Phys. Rev. B **8**, 5632 (1973).
[20] S. Sze and K. K. Ng, *Physics of Semiconductor Devices*, 3rd ed. (Wiley, New York, 2007).
[21] S. Baroni, S. de Gironcoli, A. Dal Corso, and P. Giannozzi, Rev. Mod. Phys. **73**, 515 (2001).
[22] S. Poncé, E. R. Margine, C. Verdi, and F. Giustino, Comput. Phys. Commun. **209**, 116 (2016).
[23] P. Giannozzi, O. Andreussi, T. Brumme, O. Bunau, M. B. Nardelli, M. Calandra, R. Car, C. Cavazzoni, D. Ceresoli, M. Cococcioni, N. Colonna, I. Carnimeo, A. D. Corso, S. de Gironcoli, P. Delugas, R. DiStasio, A. Ferretti, A. Floris, G. Fratesi *et al.*, J. Phys.: Condens. Matter **29**, 465901 (2017).
[24] A. A. Mostofi, J. R. Yates, G. Pizzi, Y.-S. Lee, I. Souza, D. Vanderbilt, and N. Marzari, Comput. Phys. Commun. **185**, 2309 (2014).
[25] F. Giustino, M. L. Cohen, and S. G. Louie, Phys. Rev. B **76**, 165108 (2007).
[26] N. Marzari, A. A. Mostofi, J. R. Yates, I. Souza, and D. Vanderbilt, Rev. Mod. Phys. **84**, 1419 (2012).
[27] See Supplemental Material at http://link.aps.org/supplemental/10.1103/PhysRevB.97.121201 for further details on the methodology, as well as Figs. S1–S5 and Tables S1–S4.
[28] D. M. Ceperley and B. J. Alder, Phys. Rev. Lett. **45**, 566 (1980).
[29] J. P. Perdew and A. Zunger, Phys. Rev. B **23**, 5048 (1981).
[30] J. P. Perdew, K. Burke, and M. Ernzerhof, Phys. Rev. Lett. **77**, 3865 (1996).
[31] D. R. Hamann, Phys. Rev. B **88**, 085117 (2013).
[32] P. Y. Yu and M. Cardona, *Fundamentals of Semiconductors*, edited by H. E. Stanley and W. T. Rhodes (Springer, New York, 2010).
[33] A. Marini, C. Hogan, M. Grüning, and D. Varsano, Comput. Phys. Commun. **180**, 1392 (2009).
[34] F. J. Morin and J. P. Maita, Phys. Rev. **96**, 28 (1954).
[35] R. A. Logan and A. J. Peters, J. Appl. Phys. **31**, 122 (1960).
[36] G. W. Ludwig and R. L. Watters, Phys. Rev. **101**, 1699 (1956).
[37] C. Jacoboni, C. Canali, G. Ottaviani, and A. A. Quaranta, Solid-State Electron. **20**, 77 (1977).
[38] H. Brooks, Phys. Rev. **83**, 879 (1951).
[39] S. S. Li and W. R. Thurber, Solid-State Electron. **20**, 609 (1977).
[40] M. S. Hybertsen and S. G. Louie, Phys. Rev. B **35**, 5585 (1987).
[41] R. Resta, Phys. Rev. B **16**, 2717 (1977).
[42] See http://people.sissa.it/-pl2X-sim-dalcorso/thermo_pw_dist.html.
[43] S. Poncé, Y. Gillet, J. Laflamme Janssen, A. Marini, M. Verstraete, and X. Gonze, J. Chem. Phys. **143**, 102813 (2015).
[44] D. C. Cronemeyer, Phys. Rev. **105**, 522 (1957).
[45] J. Dorkel and P. Leturcq, Solid-State Electron. **24**, 821 (1981).
[46] J. Bardeen and W. Shockley, Phys. Rev. **80**, 72 (1950).
[47] F. J. Blatt, Solid State Phys. **4**, 199 (1957).
[48] R. W. Keyes, J. Appl. Phys. **30**, 454 (1959).
[49] J. Ma, A. S. Nissimagoudar, and W. Li, Phys. Rev. B **97**, 045201 (2018).
[50] See http://doi.org/10.5281/zenodo.22558.